2026 IEEE International Conference on Robotics and Automation (ICRA 2026)
June 1-5, 2026. Vienna, Austria

Trajectory Optimization Through Mixed-Integer Optimization of Contact Dynamics for Switching End Effector Locomotion

Jared Morgan, Mahdi Agheli

***Abstract*— Trajectory optimizers for legged robots typically assume a single end effector on each leg, often a foot or wheel, without switching to another. Robots employing point-modeled end effectors, compared to those with wheeled end effectors, often benefit in adaptability and maneuverability but at the cost of higher energy expenditure and lower speed. While current hardware supports switching between these two end-effector types, existing research has largely focused on maintaining stability during switching, with little attention to determining when each type is most effective. To our knowledge, this paper introduces the first framework that simultaneously optimizes both trajectories and end-effector contact dynamics through mixed-integer optimization. We validate our approach by solving and executing trajectories with a whole-body controller in Gazebo across a variety of terrains, including ramps and stepping stones. The results show that our framework not only handles diverse terrains but also exploits contact dynamics to reduce cost of transport and increase speed compared to foot-only locomotion.**

I. Introduction

Legged robots have emerged as promising platforms for mobility and manipulation in complex, unstructured environments. Their performance, however, can be heavily influenced by the design of the End Effector (EE) interacting with the terrain. The EE dynamics affect locomotion efficiency, stability, and adaptability, yet no single design provides an ideal solution across all conditions. As a result, design and selection of optimal EE as well as identifying and leveraging the strengths of different EE types remains an open challenge in legged robotics.

For legged robots, two dominant paradigms exist: point-contact feet [1], [2] and wheeled EEs [3], [4]. Point-contact feet offer versatility, agility, and simpler low-dimensional control, particularly on irregular or cluttered terrain [5]. By contrast, wheels excel on flat or moderately structured surfaces, where rolling contact provides significant reductions in cost of transport [3]. In practice, many real-world environments contain both structured and unstructured regions, making it difficult for a robot limited to a single end-effector type to achieve both efficiency and adaptability.

This observation has motivated initial explorations into hybrid or reconfigurable systems [6], including mechanisms that allow switching between wheels and feet. For example, [7] introduced a parallel switching mechanism with a state-machine controller. [8] introduced a design to quickly change contact dynamics by changing the knee configuration. However, while these works demonstrate the feasibility of switching, little research has addressed how to plan motion that fully exploits both modalities and optimizes across their distinct contact dynamics. [9] permits wheel or feet end effectors but only with a linear relationship between dynamics, actuated wheel speed in this case, and is not generalizable to other end effectors. [10] optimizes foot contact time to show that linear variables associated with discrete variables can be optimized in real-time. This does not optimize the discrete variable directly making it unfit for EE optimization. This gap motivates the approach presented in this paper.

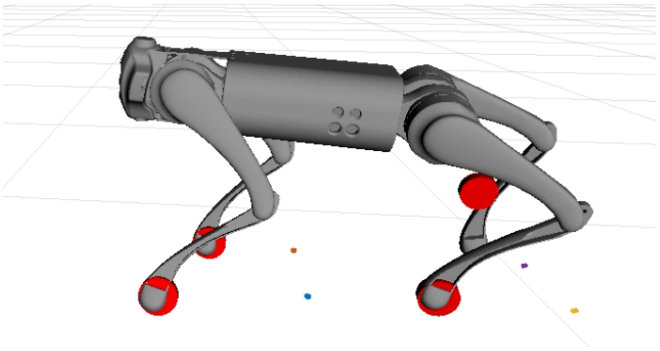

Fig. 1: Simulated Quadruped with Switching Wheel-feet EEs

Switching between EEs is inherently a discrete problem, since each EE either contributes its contact dynamics or does not. In contrast, the dominant model-based approaches for legged robots rely on trajectory optimization, which is formulated as a continuous process that drives the system from an initial state to a desired state. While most solutions use a nonlinear trajectory optimizer over a limited time horizon in a framework known as model predictive control (MPC) [11], these nonlinear optimizers are generally not tractable for handling discrete mode-switching in real time. Instead, trajectory optimization approaches based on mixed-integer formulations have emerged as a way to incorporate discrete variables, such as contact decisions, directly into the optimization process [12], [13].

[14] first introduced the problem as a footstep-planning formulation, where goal distance, footstep distance, and total number of contacts are weighted to generate a plan that progresses toward the goal while remaining constrained to distinct steppable regions. [15], [16] extend the mixed-integer footstep planning approach by integrating it with nonlinear MPC. However, this decoupled strategy—separating footstep planning from body dynamics—can be problematic, as a fixed footstep plan may lead to failure when the system

Jared Morgan and Mahdi Agheli are with the Robotics Engineering Department, Worcester Polytechnic Institute, Worcester, MA 01609, USA. {jmmorgan4, mmaghelih}@wpi.edu.

dynamics change due to external factors. [13] instead extends [14] by optimizing the footstep plan jointly with the body dynamics, enabling simultaneous gait and motion planning.

However, for switching EEs, the contact type and timing highly influences the body dynamics and cannot be decoupled as simply as fixed contact dynamics. Therefore, we build on the framework introduced in [12] to optimize both contact timing and contact dynamics, enabling robot traversal that is explicitly informed by how EEs interact with the terrain.

The main contribution of this paper is the formulation of a mixed-integer quadratically constrained control problem (MIQCCP) that optimizes end-effector selection and gait based on the interaction of each EE with the terrain. To our knowledge, this is the first trajectory optimization framework that enables locomotion informed by changing contact dynamics for legged robots equipped with switching EEs. In addition, we extend existing whole-body controllers (WBC) and state-estimation frameworks to support the robust execution of the planned trajectories. Together, these developments allow robots with switchable EEs to select contact dynamics in accordance with desired behaviors. We validate the proposed methodology in Gazebo simulation on the Unitree Go1 across a variety of terrains.

The rest of the paper is organized as follows. Section II presents a novel method of trajectory optimization through EE optimization followed by WBC in Section III. Section IV covers the results of our experimental simulations with a modified Unitree Go1 and Section V concludes the paper.

II. Simultaneous Trajectory and EE Optimization

In this section we introduce our trajectory optimizer for exploiting contact dynamics through the switching of EEs.

A. Linear Centroidal Dynamics

We begin with introducing the system inputs and decision variables for the movement of the robot's Center of Mass (CoM) as a floating base. As in [12], we decouple the EE states from the state of the body's CoM and discard the leg joints to allow for a more linear representation of dynamics. The dynamics of the body state are therefore expressed as

$$m\ddot{\mathbf{x}} = m\mathbf{g} + \sum_{l=1}^{N_l} \lambda_l + \mathbf{f}_l, \tag{1}$$

which is then discretely integrated using midpoint Euler integration across N_k knot points where each knot point k contains the robot's current state and inputs. Variables are transcribed as written in TABLE I.

B. Gait and Swing Trajectory

Next, we introduce our binary swing matrix that allows the optimization of the movement of legs to stably apply force to the CoM while following its trajectory. Rather than the footstep plan model from [14], we use a binary swing matrix $\mathbf{S} \in \{0,1\}^{N_l \times N_j}$ where $S_{l,j}$ means that leg l swings during knot group j. The swing trajectories are then given by a quintic spline in the lateral directions and a septic spline in the vertical. These splines constrain the starting and ending

TABLE I: Variables in Trajectory Optimization

$\mathbf{x} = [x_1, x_2, x_3]^T$	Center of mass in the world frame
$\theta = [\theta_1, \theta_2, \theta_3]^T$	Center of mass orientation
$\mathbf{p}_l = [p_{1,l}, p_{2,l}, p_{3,l}]^T$	End-effector positions in the world frame
$\lambda_l = [\lambda_{1,l}, \lambda_{2,l}, \lambda_{3,l}]^T$	Contact forces
$\mathbf{f}_l = [f_{1,l}, f_{2,l}, f_{3,l}]^T$	Frictional forces at leg l
N_l, N_k	Number of legs and knots in trajectory
N_r, N_e	Number of regions and EE types
N_j	Number of swing knot groups
$\mathbf{U}_l^+ = [U_{l,1}^+, U_{l,2}^+, U_{l,3}^+]^T$	The upper bound of $\ddot{\theta}$ from leg l.
$\mathbf{U}_l^- = [U_{l,1}^-, U_{l,2}^-, U_{l,3}^-]^T$	The lower bound of $\ddot{\theta}$ from leg l.

acceleration to 0, allow the starting and ending velocities to be taken into account when the EE is a wheel, and allow the footsteps to be optimized. This is accomplished through the swing matrix by relating the footstep at the beginning of the swing phase to the footstep at the end of the swing phase according to a spline modeled by

$$\mathcal{S}(t) = \sum_{i}^{N} a_i t^i, \tag{2}$$

$$\mathbf{G}\mathbf{a} = \mathbf{g}, \tag{3}$$

$$\mathbf{g}_q = [\mathbf{p}_0, \mathbf{v}_0, \mathbf{0}, \mathbf{p}_f, \mathbf{v}_f, \mathbf{0}]^T, \tag{4}$$

$$\mathbf{g}_s = [\mathbf{p}_0, \mathbf{v}_0, \mathbf{0}, \mathbf{p}_f, \mathbf{v}_f, \mathbf{0}, \mathbf{p}_{1/2}, \mathbf{0}]^T, \tag{5}$$

$$\mathbf{S}_{l,j} = 1 \implies \mathbf{p}_{l,k} = \mathcal{S}\left(\frac{k}{\rho} - j\right), \tag{6}$$

where ρ is the number of knots per knot grouping j, $\implies$ is the implication operator used to constrain other variables according to binary variables using big-M format, and $\mathbf{A}$ is a precomputed matrix that linearly relates the EE's starting position $\mathbf{p}_0$, starting velocity $\mathbf{v}_0$, landing position $\mathbf{p}_f$, and landing velocity $\mathbf{v}_f$ as in subsection II-D. $\mathbf{a}_q$ denotes the vector of desired starting and ending positions, velocities, and accelerations for a quintic spline and $\mathbf{a}_s$ adds the desired swing height and zero velocity at the swing apex. $\mathbf{b}(t)$ then defines the parametric curve that models the spline from the lifting position to the ending position where t is the percentage time of the total swing phase duration. The implication notably leaves the positions of the starting and landing footsteps unconstrained, allowing them to be optimized passively rather than as part of a footstep plan. Additionally, because force cannot be applied on the terrain during a swing, the implication

$$\mathbf{S}_{l,j} = 1 \implies \lambda_{l,k} = 0 \quad \forall k = [\rho j, \rho(j+1)), \tag{7}$$

is also applied to ensure the plan does permit the application of force during the swing phase. Fig. 2 visualizes how the binary matrix constrains a foot trajectory.

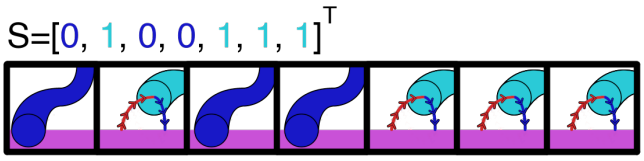

Fig. 2: Swing Matrix Effects on Locomotion for One Leg

C. Angular Centroidal Dynamics

Here we introduce the method we employ for convexly minimizing angular acceleration. The angular dynamics are more complex, as they are typically nonlinear, represented in the form

$$\mathbf{I}\ddot{\theta} = \sum_{l=1}^{N_l} (\mathbf{x} - \mathbf{p}_l) \times \lambda_l, \tag{8}$$

where $\mathbf{I}$ is the mass-moment matrix. However, this bilinear relationship is notably non-convex and significantly increases computation time for mixed-integer problems. [17] introduces a difference of convex functions decomposition that allows an upper bound on angular momentum, $\mathbf{U}^+$, and a lower bound, $\mathbf{U}^-$, to lie on the bilinear manifold that is revealed in the expansion of eq. (8) that includes the upper and lower bounds in the cost function of the trajectory optimizer such that at every timestep the solver aims to find

$$\min_{(\mathbf{x}-\mathbf{p}_l),\lambda_l} \quad \sum_{l=1}^{N_l} \mathbf{U}^+{}_l + \mathbf{U}^-{}_l, \quad \sum_{l=1}^{N_l} \frac{1}{4}(\mathbf{U}^+{}_l - \mathbf{U}^-{}_l) = \mathbf{I}\ddot{\theta}. \tag{9}$$

It can then be observed that this allows the angular acceleration to be tracked. This does not, however, necessarily allow the angular acceleration to be minimized because while $\min_{(\mathbf{x}-\mathbf{p}_l),\lambda_l} \mathbf{U}^+{}_l + \mathbf{U}^-{}_l$ and $\min_{(\mathbf{x}-\mathbf{p}_l),\lambda_l} \mathbf{U}^+{}_l - \mathbf{U}^-{}_l$ occur at the same set $(\mathbf{x}-\mathbf{p}_l), \lambda_l$, $\min_{(\mathbf{x}-\mathbf{p}_l),\lambda_l} \sum_{l=1}^{N_l} \mathbf{U}^+{}_l + \mathbf{U}^-{}_l$ and $\min_{(\mathbf{x}-\mathbf{p}_l),\lambda_l} \sum_{l=1}^{N_l} \mathbf{U}^+{}_l - \mathbf{U}^-{}_l$ do not. [12] avoids the divergence from optimal angular acceleration that can occur when performing complex actions by limiting the robot to simple actions. While approaches such as [18]'s McCormick Envelopes and [9]'s ZMP constraints may be more accurate, they are also computationally more expensive. Instead, this work leverages mixed-integer programming to develop a heuristic that optimizes the CoM towards the centroid of the foot contact locations during swing phases, allowing for the execution of more complex motions that are more recoverable by the WBC. The centroid of the foot contacts can be expressed as the sum of all the foot locations divided by the total number of feet in contact. In mixed integer form, this is expressed as

$$\mathbf{S}_{l,j} = 0 \implies \upsilon_{l,k} = \mathbf{p}_{l,k}, \tag{10}$$

$$\mathbf{S}_{l,j} = 1 \implies \upsilon_{l,k} = 0, \tag{11}$$

$$\sum_{l=1}^{N_l} \mathbf{S}_{l,j} = n \implies \mathbf{c}_k = \frac{\sum_{l=1}^{N_l} \upsilon_{l,k}}{(N_l - n)}, \tag{12}$$

where $\upsilon_{l,k} \in \mathbb{R}^3$ represents the vertex of the foot contact polygon for leg l, $\mathbf{c_k}$ represents the centroid of the foot contact polygon, and where eq. (12) is modeled by decomposing the swing sum into binary variables

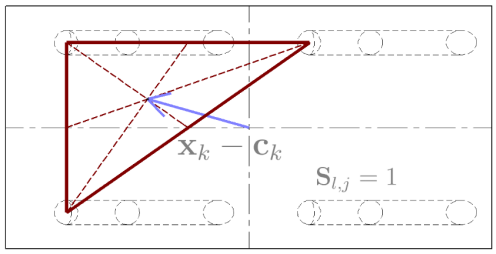

Fig. 3: Contact Polygon Centroid and CoM Displacement

$$\sum_{l=1}^{N_l} \mathbf{S}_{l,j} = \sum_{l=1}^{N_l} l s_{l,j}, \tag{13}$$

$$\sum_{l=1}^{N_l} s_{l,j} = 1, \tag{14}$$

$$s_{l,j} = 1 \implies \mathbf{c}_k = \frac{\mathbf{v_k}}{(N_l - l)}, \tag{15}$$

where $s_{l,j}$ represents an auxiliary binary variable that, when multiplied by l, is equal to 1 only when l legs are swinging. Fig. 3 demonstrates the displacement between the centroid and the position of the CoM that is minimized to allow the WBC to better control angular acceleration.

D. Region Assignment and Contact Dynamics

We introduce the binary dynamics matrix that allows for the optimization of contact dynamics based on terrain and EE interaction. To optimize over contact dynamics, we first encode the contact dynamics in the binary matrix $D \in \{0,1\}^{N_l \times N_j \times N_r \times N_e}$ where N_r is the number of safe regions and N_e is the number of EEs being optimized over. We first restrict the ability to switch EEs exclusively to swing phases to limit unmodeled interference of a switching mechanism. This is modeled with a single implication that forces the dynamics of a leg l to remain the same when the leg has not swung and remain optimizable when the leg is swinging, expressed as

$$\mathbf{S}_{l,j} = 0 \implies \mathbf{D}_{l,j,r,e} = \mathbf{D}_{l,j-1,r,e} \quad \forall j > 1, \tag{16}$$

We constrain that all legs must have exactly one set of EE dynamics at a given time by

$$\sum_{r=1}^{N_r} \sum_{t=1}^{N_e} \mathbf{D}_{l,j,r,e} = 1 \quad \forall j = [1, N_j], l = [1, N_l]. \tag{17}$$

The effects that contact dynamics have on EE motion, contact forces, safe region assignment, and body dynamics are explored in sections II-D.1-II-D.4 and written simply as

$$\mathbf{S}_{l,j} = 0 \& \mathbf{D}_{l,j,r,e} = 1 \quad \implies \quad \mathcal{D}(r,e), \tag{18}$$

where $\mathcal{D}(r,e)$ are the set of dynamics and constraints that arise from the interaction between region r and EE type t as applied to leg l during knot segment j.

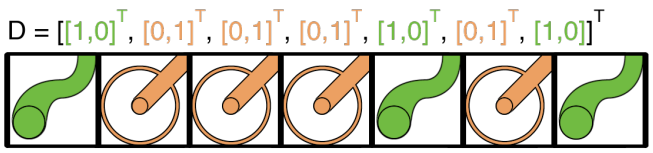

Fig. 4: The Dynamics Matrix Effects on Locomotion with One Region, One Leg, and Two EE Types

1) End Effector Motion: The motion of an EE can be modeled based on the terrain and the EE type. For a foot, motion is undesirable as it is generally unstable and represents the applied forces are not entirely transferred to the body. Therefore we constrain

$$\mathcal{D}(r,1) \leftarrow \mathbf{p}_k = \mathbf{p}_{k-1} \quad \forall k = [\rho j, \rho(j+1)), \tag{19}$$

which models that a foot is in the same position at knot point k as it was at knot point $k-1$ when $e=1$ represents the leg has a footed contact and $e=2$ represents the leg has a wheeled contact. Assuming wheels may move freely in the rolling direction, corresponding with the robot's forward direction, so we constrain

$$\mathcal{D}(r,2) \leftarrow \mathbf{p}_{1,k} = \mathbf{p}_{1,k-1} + \int_{k-1}^{k} \dot{\mathbf{x}}_1, \tag{20}$$

$$\mathcal{D}(r,2) \leftarrow \mathbf{p}_{2,k} = \mathbf{p}_{2,k-1}, \tag{21}$$

where $\dot{x}_1$ corresponds to the forward body velocity. This constraint therefore models that the forward direction position of the EE at knot k changes according the integration of the body velocity. Fig. 4 demonstrates how the dynamics matrix constrains EE types.

2) Region Assignment: Because we are not optimizing a footstep plan, we need another method to force footsteps onto a safe convex plane. We accomplish this by constraining the EE at all times to lie on the convex plane r by

$$\mathcal{D}(r,1) \leftarrow \mathbf{A}_r\mathbf{p} \leq \mathbf{b}_r, \tag{22}$$

as in [14]. This assumption no longer holds true for wheels which can cross continuous convex planes. By grouping all continuous convex planes into ζ_r, we can then model the rolling region assignment as

$$\mathcal{D}(r,2) \leftarrow \bigcup_{\eta \in \zeta_r} \mathbf{A}_\eta\mathbf{p} \leq \mathbf{b}_\eta, \tag{23}$$

and allow wheels to cross the continuous convex planes that compose ζ_r. The union of the convex planes is optimized using binary variables $z_\eta \in \{0,1\}$ and big-M formulation as

$$\mathbf{A}_\eta\mathbf{p} \leq \mathbf{b}_\eta + Mz_\eta, \tag{24}$$

$$\sum_{\eta=1}^{\zeta} z_\eta \leq \zeta - 1. \tag{25}$$

Fig. 5 shows the effects of the dynamics matrix's region assignment for a single leg and a single EE type.

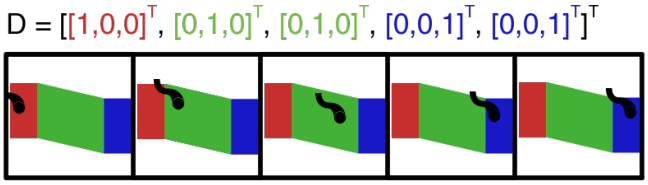

Fig. 5: The Dynamics Matrix Effects on Locomotion with Three Regions, One Leg, and One EE Type

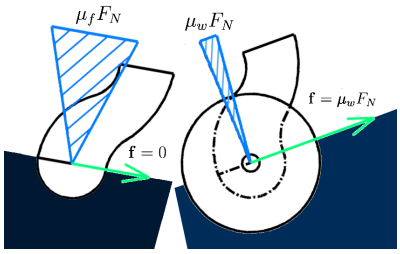

Fig. 6: Friction Cone and Frictional Force for Legs vs Wheel

3) Contact Forces: Given a convex plane r with surface normal $\hat{n}$ and a basis defined by vectors $\hat{t}$ and $\hat{b}$ where we arbitrarily determine $\hat{t}$ to be in the wheel's rolling direction, we can constrain the applied forces to lie within linearized friction cones of both point feet and wheels based on the coefficient of friction. Using [19]'s representation, we model friction by

$$\left.\begin{aligned} \lambda \cdot \hat{n} &\geq 0 \\ |\lambda \cdot \hat{t}| &\leq \mu_{r,e,\hat{t}}(\lambda \cdot \hat{n}) \\ |\lambda \cdot \hat{b}| &\leq \mu_{r,e,\hat{b}}(\lambda \cdot \hat{n}) \end{aligned}\right\} = \mathcal{F}(r,e), \tag{26}$$

where $\mu_{r,t,\hat{t}}$ is the friction between the material associated with plane r and the material associated with EE e in the direction $\hat{t}$ while $\mu_{r,t,\hat{b}}$ is the same interaction but in the orthogonal direction. This can then be made optimizable by

$$\mathcal{D}(r,e) \leftarrow \mathcal{F}(r,e). \tag{27}$$

It can be observed that these constraints adequately model the acceptable reaction forces for a convex plane that could be applied without slipping. Moreover, because the rolling friction of a wheel is significantly smaller in the rolling direction, the reaction forces are constrained such that the body will accelerate as the wheel rolls down a slope and remain stationary relative to the body on flat terrain. Fig. 6 demonstrates the difference in friction cones between the two EE types.

4) Rolling Friction: Assuming the same basis $\hat{t}$ defines the rolling direction, frictional forces along $\hat{t}$ will decelerate the body if the EE is a wheel. This can be modeled in the dynamic matrix by

$$\mathcal{D}(r,1) \leftarrow \mathbf{f}_l = 0, \tag{28}$$

$$\mathcal{D}(r,2) \leftarrow \mathbf{f}_l = \mu_{r,2}\frac{\lambda \cdot \hat{n}}{||\hat{n}||^2}\hat{t}, \tag{29}$$

constraining the rolling frictional force to be none for feet and the coefficient of friction magnitude of the reaction force projected onto the surface normal and mapped onto the rolling direction. This models the mapping of $F_{fr} = \mu F_N$ into 3d vector space.

E. Reachability Constraints

Here, we explain how to keep EEs within executable distances of the body. Reachability constraints relate EEs to the location and orientation of the body. Reachability of a kinematic chain is difficult to compute, especially as it relates to the body and the other legs. Because of this and because the relationship is nonconvex, we represent reachability using a simplified representation as in [14]. Finding it suitable for our purposes and because there are already so many indicator constraints that slow the solver, we omit the piecewise representations of sine and cosine in favor of the inscription of the reachable circle by

$$(\mathbf{x} - \mathbf{p}_l)^- \leq (\mathbf{x} - \mathbf{p}_l) \leq (\mathbf{x} - \mathbf{p}_l)^+, \tag{30}$$

where $(\mathbf{x} - \mathbf{p}_l)^-$ represents the lower bound of the distance between the body and the EE and $(\mathbf{x} - \mathbf{p}_l)^+$ represents the upper bound. These constraints allow the feet to move freely while swinging but not exceed reasonably reachable configurations.

F. Trajectory Optimization

With the above constraints, we build the cost function that defines our trajectory optimization as

$$\min_{\ddot{\mathbf{x}},\lambda,\mathbf{U}^+,\mathbf{U}^-,S} \quad \Phi + \sum_{k=1}^{N_k} \phi(k) + w_s \sum_{l=0}^{N_l} \sum_{j=0}^{N_j} \mathbf{S}_{l,j} j, \tag{31}$$

where $\Phi(\mathbf{z}_{obj})$ draws the final solution to the desired state $\mathbf{z}_{obj}$ as defined by

$$\Phi = \begin{bmatrix} ||\mathbf{x} - \mathbf{x}_d||_{Q_x} \\ ||\theta - \theta_d||_{Q_\theta} \end{bmatrix}, \tag{32}$$

where z_v represents the desired ending value of state v. $||v||_{Q_v}$ represents the weighted squared L-2 norm expressed as $v^T Q_v v$. $w_s \sum_{l=0}^{N_l} \sum_{j=0}^{N_j} S_{l,j} j$ encourages the minimization of steps by penalizing swings directly. Later steps are penalized more heavily which encourages solutions that bring the footsteps to their final states more quickly. The running cost

$$\begin{aligned} \phi(k) = ||\ddot{\mathbf{x}}_k||_{Q_a} + ||\lambda_k||_{Q_\lambda} + \\ w_{U^+} \mathbf{U}_k^+ + w_{U^-} \mathbf{U}_k^- + ||\mathbf{x}_k - \mathbf{c}_k||_{Q_c}, \end{aligned} \tag{33}$$

minimizes the body acceleration $\ddot{\mathbf{x}}$, the applied contact force $\ddot{\lambda}$, the contribution of each EE to angular dynamics $\mathbf{U}^+ + \mathbf{U}^-$, and the divergence from the foot contact polygon $\mathbf{x}_k - \mathbf{C}_k$. Q_c allows for a tunable constant that weights how strictly a generated trajectory adheres to the centroid of the foot contacts.

III. Whole Body Control and State Estimation

This work introduces a novel wheel-footed WBC extending [4], [20]–[22] that allows for execution of both footed and wheeled trajectories according to the dynamics plan output by the trajectory optimizer. As in [13], we correct the relationship between the desired state $\mathbf{x}_d, \dot{\mathbf{x}}_d, \ddot{\mathbf{x}}$ and the measured state $\mathbf{x}, \dot{\mathbf{x}}$ through a PD controller as

$$\ddot{\mathbf{z}}_r = \ddot{\mathbf{z}}_d + K_z (\mathbf{z}_d - \mathbf{z}) + D_z (\dot{\mathbf{z}}_d - \dot{\mathbf{z}}), \tag{34}$$

where $\mathbf{z} = [\mathbf{x}, \theta]^T$. We also add a PD controller for the rolling wheel's reference acceleration through

$$\ddot{\mathbf{w}}_r = K_w (\mathbf{w}_d - \mathbf{w}) + D_w (\dot{\mathbf{w}}_d - \dot{\mathbf{w}}), \tag{35}$$

and the swing foot reference acceleration

$$\ddot{\mathbf{s}}_r = K_s (\mathbf{s}_d - \mathbf{s}) + D_s (\dot{\mathbf{s}}_d - \dot{\mathbf{s}}). \tag{36}$$

Expanding on [22], we model the equations of motion as

$$\mathbf{M}\ddot{\mathbf{q}} + \mathbf{h} = \mathbf{S}\tau + \mathbf{J}_f^T \lambda_f + \mathbf{J}_w^T \lambda_w. \tag{37}$$

Where $\mathbf{J}_f^T \in \mathbb{R}^{n_f \times (6+n)}$ is the Jacobian matrix of the feet contacts, $\mathbf{J}_w^T \in \mathbb{R}^{n_w \times (6+n)}$ is the Jacobian of the wheeled contacts, and where n_f is the number of footed contacts and n_w is the number of wheeled contacts.

We then aim to solve for $\mathbf{u}^* = [\ddot{\mathbf{q}}^*, \lambda^*, \tau^*]^T$ where $\ddot{\mathbf{q}}^* \in \mathbb{R}^{3N_l}$ represents the vector optimized of joint accelerations, $\lambda^* \in \mathbb{R}^{3N_l}$ represents the vector of optimized contact forces, and $\tau^* \in \mathbb{R}^{3N_l}$ represents the vector of optimized joint torques. We solved for these inputs as a quadratic program by

$$\begin{aligned} \mathbf{u}^* = \underset{\mathbf{u}=[\ddot{\mathbf{q}},\lambda,\tau]^T}{\arg\min} \quad & ||\ddot{\mathbf{z}} - \ddot{\mathbf{z}}_r||_{Q_z} + \\ & ||\mathbf{J}_{wu}\ddot{\mathbf{q}} + \dot{\mathbf{J}}\dot{\mathbf{q}} - \ddot{\mathbf{w}}_r||_{Q_w} + \\ & ||\mathbf{J}_{sw}\ddot{\mathbf{q}} + \mathbf{J}_{sw}\dot{\mathbf{q}} - \ddot{\mathbf{s}}_r||_{Q_s}, \end{aligned} \tag{38}$$

$$s.t.$$

$$\text{(Dynamics)} \quad \mathbf{M}\ddot{\mathbf{q}} + \mathbf{h} = \mathbf{S}\tau + \mathbf{J}_w^T \lambda + \mathbf{J}_f^T \lambda, \tag{39}$$

$$\text{(Stationary feet)} \quad \mathbf{J}_f \ddot{\mathbf{q}} + \dot{\mathbf{J}}_f \dot{\mathbf{q}} = \mathbf{0}, \tag{40}$$

$$\text{(Fixed wheel)} \quad \mathbf{J}_{wl} \ddot{\mathbf{q}}_l + \dot{\mathbf{J}}_{wl} \dot{\mathbf{q}}_l = \mathbf{0}, \tag{41}$$

$$\text{(Friction cone)} \quad \mathbf{P}_w \lambda_w \leq \mathbf{r}, \quad \mathbf{P}_f \lambda_f \leq \mathbf{r}, \tag{42}$$

$$\text{(Torque Limits)} \quad \underline{\tau} \leq \tau \leq \bar{\tau}, \tag{43}$$

where $\mathbf{J}_{wu}$ is the portion of the Jacobian that applies in the rolling direction and $\mathbf{J}_{wl}$ is the portion that does not. As in [22] we then encode these costs and constraints for optimization in the form $||\mathbf{G}\mathbf{u} - \mathbf{g}_0||$, $\mathbf{A}\mathbf{u} = \mathbf{b}$, $\mathbf{C}\mathbf{u} \leq \mathbf{d}$.

While WBC converts trajectories into torques which are then executed, state estimation informs the robot of its current state for WBC to optimize. State estimators such as [23] rely on the change in position, as calculated by the forward leg kinematics, of the EEs for the correction step of an extended Kalman filter. Without a change of the EEs in the body frame, the correction step corrects away its forward velocity. To amend this we added the approximation

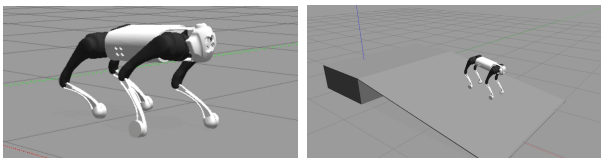

(a) Flat Terrain (b) Downward Ramp

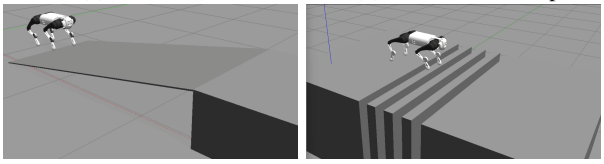

(c) Upward Ramp (d) Stepping Stones

Fig. 7: Experimental Setups: Different Terrains for Testing

of robot's body velocity to the EE velocity in the body frame when it was a wheel in the form

$$\mathbf{C}\hat{\mathbf{x}} = (\mathbf{x} - \mathbf{p}) + \mathbf{W}\mathbf{v}, \tag{44}$$

where $\mathbf{W} \in \mathbb{R}^{3N_l}$ and $\mathbf{W}_l = [1, 0, 0]^T$ when the EE is a wheel and $[0, 0, 0]^T$ when the EE is a foot. This allows the state estimation to have the benefits of correction from leg odometry and understand its motion while rolling.

IV. Experimental Results

Our approach was validated on the Unitree Go1 quadruped robot by performing simulations in Gazebo multi-robot simulator version 11.15.1 using the Open Dynamics Engine with an artificial 9 millisecond delay between commanded torques and simulated actuation. The switching mechanism was modeled as nearly instant during the swing phase with light wheels that effect leg inertia. We employ Gurobi version 12 as the mixed-integer optimizer. All computation benchmarks are performed on an *Intel Core Ultra 7 115H* processor. The method was tested on a variety of terrains as shown in Fig. 7.

A. End Effector and Gait Selection

We demonstrate in our experiments the ability to optimize gait and EE selection to minimize the associated cost functions and remain within region limits. Our proposed method allows the robot to traverse multiple terrains according to the interactions of the EEs with the terrain.

1) Flat Ground without Friction: On flat ground, our method demonstrates the ability to minimize swings, contact force, and time to reach goal position by optimizing walking in favor of wheels. Starting with feet, the optimizer switches all legs to wheels early in the trajectory, minimizing contact force. Once the rolling has brought the robot to its goal state, one leg is returned to a foot to bring the robot to a stop, minimizing swing phases. The three wheeled EEs also experimentally improve the robot's ability to adjust its position toward the goal state through the WBC, with the single foot serving as a base to correct for unplanned differences in rolling velocity. Fig. 8 shows the gait diagram for a 4.5 second trajectory on flat ground with green representing the foot contact and orange representing the wheel contact.

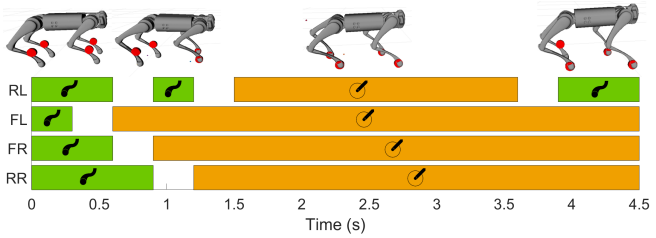

Fig. 8: Gait and EE Selection on Flat Ground with no Friction

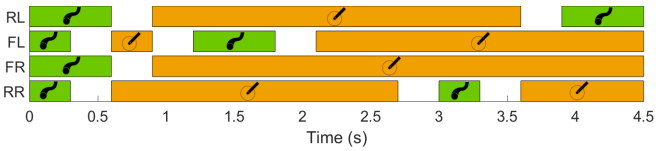

Fig. 9: Gait and EE Selection on Flat Ground with Friction

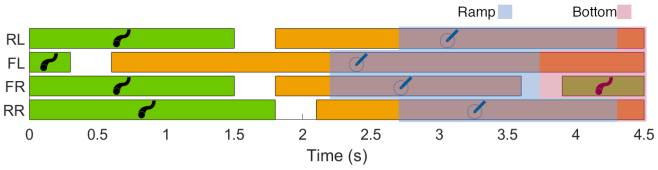

Fig. 10: Gait and EE Selection on a Downward Ramp

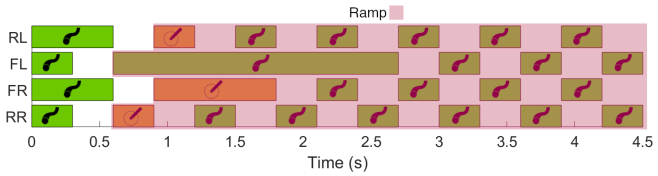

Fig. 11: Gait and EE Selection on an Upward Ramp

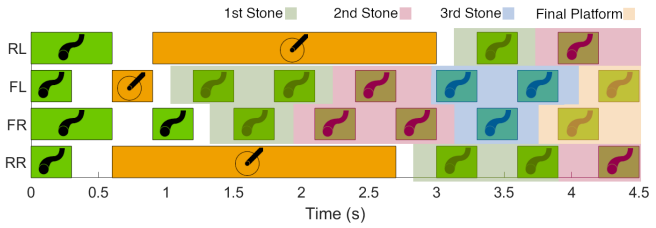

Fig. 12: Gait and EE Selection across Stepping Stones

2) Flat Ground with Friction: On the flat ground with friction, we were able to validate both our friction model and its effects on the ability to minimize swings. The gradual decrease in velocity due to friction while rolling requires the robot to make more footed contacts to generate more force through a push leg. Fig. 9 demonstrates this by showing more foot contacts relative to Fig. 8 throughout the trajectory while most contacts remain wheels.

3) Downward Ramp: It would be expected that a contact dynamics optimizer would prefer the use of passive wheels on terrain that is slanted downward because it allows the effortless continued rolling, even with rolling friction modeled. Our results agree with this expectation. The robot approaches the ramp, switches to wheels to roll down the ramp, and then

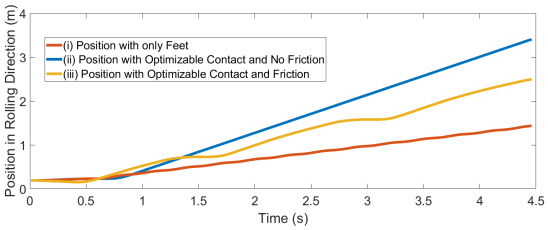

Fig. 13: Desired Trajectory on Flat Ground for Fixed Dynamics and Optimizable Dynamics (with and without Friction).

switches back at the end of the ramp to come to a complete stop using a foot. Fig. 10 demonstrates the behavior when the wheels are able to *roll* across the convex planes belonging to the same continuous group as in eq. (23). Without the grouping of convex planes, the gait would be forced to execute a *swing* phase to cross from the platform to the ramp.

4) Upward Ramp: Unlike the downward ramp, it cannot be expected passive wheels would be optimal on an upward ramp because wheels cannot apply force up the ramp. Our results confirm this expectation but also show that it is optimal in some cases, particularly at the beginning of the ramp, to use a combination of feet and wheels to gain speed and switch to all feet once wheels lose forward velocity. Fig. 11 demonstrates an trajectory where this is seen.

5) Stepping Stones: For the stepping stones, the contacting wheels would roll onto the gap because they move with the body's velocity. Therefore, the optimizer selects to use feet on the areas where rollable space is limited to prevent wheels from rolling into unpermitted terrain. This is demonstrated in Fig. 12 which shows the gait across the stepping stones spaced 20cm apart. The robot's maximum stepping distance is 50cm.

B. Trajectory Generation and Speed

A key advantage of wheels over feet is their potential for faster locomotion through extended rolling contact, which reduces the need for frequent stepping discontinuities (see Fig. 8 for example). We evaluate our framework's ability to exploit this advantage in gait generation under three flat-ground conditions: (i) non-optimizable EEs restricted to feet, (ii) optimizable EEs without friction modeling (Fig. 8), and (iii) optimizable EEs with friction modeling Fig. 9. All cases are assigned the same unreachable goal state and optimize a trajectory over 4.5 seconds. Fig. 13 shows the resulting trajectories. We find that, regardless of friction modeling, our method exploits the speed advantage of wheels: in 4.5 seconds, the foot-only robot covers 1.43 m, whereas with feet and wheels it reaches 2.5 m with friction and 3.4 m without friction. This indicates that the robot with wheels reached average speeds of 0.56 m/s (74% faster) with friction modeled and 0.76 m/s (137% faster) without friction, compared to 0.32 m/s for foot-only locomotion.

C. Cost of Transport

One of the major constraints of legged robots is their power consumption. Previous works have demonstrated the ability of wheel-legged robots to decrease power consumption often using cost of transport, a unitless measure of performance, as a surrogate. We employ the method from [3] to calculate the cost of transport. Our measurements on flat ground demonstrate that, through minimization of contact forces and CoM accelerations, our optimizer is able to select EEs that minimize cost of transport. For a 9-second trajectory on flat ground, our optimizer selects EEs and gaits that yield a cost of transport of 0.105. Under the same conditions, but with optimization restricted to feet, the cost of transport increases to 0.237. This corresponds to a 55.7% reduction (≈2.3× improvement). Thus, our method, which minimizes applied force, also achieves lower cost of transport. We opt not to compare this against other methods because no methods we know of are capable of optimizing contact dynamics to generate these types of gates.

TABLE II: Average Computation Time without Friction or Multi-Region Constraint

Seconds	Terrain	N_r	N_e	N_j	Computation Time (s)
1.5	Flat	1	1	5	0.714
3	Flat	1	1	10	4.637
1.5	Flat	1	2	5	1.723
3	Flat	1	2	10	673.58
1.5	Down Ramp	3	1	5	0.977
3	Down Ramp	3	1	10	204.37
1.5	Down Ramp	3	2	5	3.887

D. Computation Benchmarking

We ran experiments across a variety of terrains and measured computation times. TABLE II reports results for flat and downhill terrains without rolling friction or multi-region constraints. As expected, because mixed-integer optimization is NP-hard, computation time increases significantly with the number of binary variables N_r, N_e, and N_j. Additional experiments revealed further increases in computation time when rolling friction or multi-region constraints were included.

Although our method demonstrated robustness across different terrains, the resulting computation times present challenges for deployment in an MPC context, where trajectories must be recalculated rapidly. However, as shown in the first row of TABLE II, our method computed a 1.5-second trajectory with five swing slots in 0.714 seconds, suggesting that for certain tasks, such as flat-terrain locomotion, our approach may still be feasible within an MPC framework. Nonetheless, the results demonstrate that our method can explicitly handle switching contact dynamics which cannot be executed using traditional nonlinear optimization methods.

V. Conclusions

We introduced and evaluated a novel mixed-integer optimization framework that simultaneously optimizes trajectories and contact dynamics, enabling robots to generate gaits that strategically exploit terrain interactions. To our knowledge, this is the first optimization approach to integrate end-effector selection into trajectory generation. We validated our approach through a variety of terrains. Experiments across

flat ground, slopes, and stepping-stone terrains demonstrated the robustness and versatility of the optimizer, which consistently selected effective end-effector combinations to ensure stable execution. On flat ground, our framework leveraged the speed advantage of wheels: robots with switching end effector showed 74% increase in speed with friction modeled and 137% increase without friction, compared to the robot speed for foot-only locomotion. In addition, our method achieved a 57% reduction in cost of transport compared to conventional legged locomotion, underscoring its potential for improved energy efficiency. Although computational demands increased in more complex terrains due to the need to manage binary contact switches, this trade-off reflects the richer modeling of contact dynamics that traditional nonlinear trajectory optimization methods cannot capture.

In future work, we aim to extend our framework to hardware implementation, addressing hardware design considerations and execution of optimized trajectories on a physical quadruped. Our current formulation limits wheel motion to a single direction, typically aligned with the body angle, but angle approximations in [14] may enable more complex turning motions with fixed-angle or actuated-angle wheels. Another avenue for improvement is to use the trajectories generated and realized by the WBC as baselines for learning-based methods, where our method could address exploration limitations. Recent studies, such as [24] highlight the promise of neural networks for solving mixed-integer programming problems, while [25] proposes warm-start strategies to reduce solve times. Our results on linear trajectories, where up to five swing segments can be generated in under 500 milliseconds, suggest that extending this approach toward real-time MPC may be feasible even without learning methods. Finally, consistent with [12], we recognize the need for more accurate and quick convex formulations of angular dynamics and intend to explore this in future work.

REFERENCES

[1] M. Hutter, C. Gehring, D. Jud, A. Lauber, C. D. Bellicoso, V. Tsounis, J. Hwangbo, K. Bodie, P. Fankhauser, M. Bloesch, R. Diethelm, S. Bachmann, A. Melzer, and M. Hoepflinger, "ANYmal - a highly mobile and dynamic quadrupedal robot," in *2016 IEEE/RSJ International Conference on Intelligent Robots and Systems (IROS)*. Daejeon, South Korea: IEEE, Oct. 2016, pp. 38–44.

[2] G. Bledt, M. J. Powell, B. Katz, J. Di Carlo, P. M. Wensing, and S. Kim, "MIT Cheetah 3: Design and Control of a Robust, Dynamic Quadruped Robot," in *2018 IEEE/RSJ International Conference on Intelligent Robots and Systems (IROS)*. Madrid: IEEE, Oct. 2018, pp. 2245–2252.

[3] M. Bjelonic, C. Dario Bellicoso, M. Efe Tiryaki, and M. Hutter, "Skating with a force controlled quadrupedal robot," in *2018 IEEE/RSJ International Conference on Intelligent Robots and Systems (IROS)*, 2018, pp. 7555–7561.

[4] M. Bjelonic, C. D. Bellicoso, Y. de Viragh, D. Sako, F. D. Tresoldi, F. Jenelten, and M. Hutter, "Keep rollin'—whole-body motion control and planning for wheeled quadrupedal robots," *IEEE Robotics and Automation Letters*, vol. 4, no. 2, pp. 2116–2123, 2019.

[5] V. S. Medeiros, E. Jelavic, M. Bjelonic, R. Siegwart, M. A. Meggiolaro, and M. Hutter, "Trajectory optimization for wheeled-legged quadrupedal robots driving in challenging terrain," *IEEE Robotics and Automation Letters*, vol. 5, no. 3, pp. 4172–4179, 2020.

[6] T. Liu, C. Zhang, J. Wang, S. Song, and M. Q.-H. Meng, "Towards terrain adaptablity: In situ transformation of wheel-biped robots," *IEEE Robotics and Automation Letters*, vol. 7, no. 2, pp. 3819–3826, 2022.

[7] C. Zhang, T. Liu, S. Song, J. Wang, and M. Q.-H. Meng, "Dynamic wheeled motion control of wheel-biped transformable robots," *Biomimetic Intelligence and Robotics*, vol. 2, no. 2, p. 100027, 2022.

[8] J. Chen, R. Qin, L. Huang, Z. He, K. Xu, and X. Ding, "Unlocking versatile locomotion: A novel quadrupedal robot with 4-dofs legs for roller skating," in *2024 IEEE International Conference on Robotics and Automation (ICRA)*, 2024, pp. 8037–8043.

[9] Y. de Viragh, M. Bjelonic, C. D. Bellicoso, F. Jenelten, and M. Hutter, "Trajectory optimization for wheeled-legged quadrupedal robots using linearized zmp constraints," *IEEE Robotics and Automation Letters*, vol. 4, no. 2, pp. 1633–1640, 2019.

[10] A. W. Winkler, C. D. Bellicoso, M. Hutter, and J. Buchli, "Gait and trajectory optimization for legged systems through phase-based end-effector parameterization," *IEEE Robotics and Automation Letters*, vol. 3, no. 3, pp. 1560–1567, 2018.

[11] P. Fankhauser, M. Bjelonic, C. Dario Bellicoso, T. Miki, and M. Hutter, "Robust Rough-Terrain Locomotion with a Quadrupedal Robot," in *2018 IEEE International Conference on Robotics and Automation (ICRA)*. Brisbane, QLD: IEEE, May 2018, pp. 5761–5768.

[12] B. Aceituno-Cabezas, C. Mastalli, H. Dai, M. Focchi, A. Radulescu, D. G. Caldwell, J. Cappelletto, J. C. Grieco, G. Fernandez-Lopez, and C. Semini, "Simultaneous Contact, Gait and Motion Planning for Robust Multi-Legged Locomotion via Mixed-Integer Convex Optimization," *IEEE Robotics and Automation Letters*, pp. 1–1, 2017, arXiv:1904.04595 [cs].

[13] B. Aceituno-Cabezas, H. Dai, J. Cappelletto, J. C. Grieco, and G. Fernández-López, "A mixed-integer convex optimization framework for robust multilegged robot locomotion planning over challenging terrain," in *2017 IEEE/RSJ International Conference on Intelligent Robots and Systems (IROS)*, 2017, pp. 4467–4472.

[14] R. Deits and R. Tedrake, "Footstep planning on uneven terrain with mixed-integer convex optimization," in *2014 IEEE-RAS International Conference on Humanoid Robots*, 2014, pp. 279–286.

[15] T. Corbères, C. Mastalli, W. Merkt, J. Shim, I. Havoutis, M. Fallon, N. Mansard, T. Flayols, S. Vijayakumar, and S. Tonneau, "Perceptive locomotion through whole-body mpc and optimal region selection," *IEEE Access*, vol. 13, pp. 69 062–69 080, 2025.

[16] B. Acosta and M. Posa, "Perceptive mixed-integer footstep control for underactuated bipedal walking on rough terrain," *IEEE Transactions on Robotics*, vol. 41, pp. 4518–4537, 2025.

[17] B. Ponton, A. Herzog, S. Schaal, and L. Righetti, "A convex model of humanoid momentum dynamics for multi-contact motion generation," in *2016 IEEE-RAS 16th International Conference on Humanoid Robots (Humanoids)*, 2016, pp. 842–849.

[18] A. K. Valenzuela, "Mixed-integer convex optimization for planning aggressive motions of legged robots over rough terrain," Ph.D. dissertation, Massachusetts Institute of Technology, 2016.

[19] J. C. Trinkle, J.-S. Pang, S. Sudarsky, and G. Lo, "On dynamic multi-rigid-body contact problems with coulomb friction," *ZAMM - Journal of Applied Mathematics and Mechanics / Zeitschrift für Angewandte Mathematik und Mechanik*, vol. 77, no. 4, pp. 267–279, 1997.

[20] C. Dario Bellicoso, C. Gehring, J. Hwangbo, P. Fankhauser, and M. Hutter, "Perception-less terrain adaptation through whole body control and hierarchical optimization," in *2016 IEEE-RAS 16th International Conference on Humanoid Robots (Humanoids)*, 2016, pp. 558–564.

[21] C. Mastalli, I. Havoutis, M. Focchi, D. G. Caldwell, and C. Semini, "Motion planning for quadrupedal locomotion: Coupled planning, terrain mapping, and whole-body control," *IEEE Transactions on Robotics*, vol. 36, no. 6, pp. 1635–1648, 2020.

[22] S. Fahmi, C. Mastalli, M. Focchi, and C. Semini, "Passive whole-body control for quadruped robots: Experimental validation over challenging terrain," *IEEE Robotics and Automation Letters*, vol. 4, no. 3, pp. 2553–2560, 2019.

[23] M. Bloesch, M. Hutter, M. A. Hoepflinger, S. Leutenegger, C. Gehring, C. D. Remy, and R. Siegwart, "State Estimation for Legged Robots: Consistent Fusion of Leg Kinematics and IMU," in *Robotics: Science and Systems VIII*. The MIT Press, Jul. 2013.

[24] X. Lin, G. I. Fernandez, and D. W. Hong, "Reduce: Reformulation of mixed integer programs using data from unsupervised clusters for learning efficient strategies," in *2022 International Conference on Robotics and Automation (ICRA)*, 2022, pp. 4459–4465.

[25] T. Marcucci and R. Tedrake, "Warm start of mixed-integer programs for model predictive control of hybrid systems," *IEEE Transactions on Automatic Control*, vol. 66, no. 6, pp. 2433–2448, 2021.